ISSN (Print) 1226-1750
ISSN (Online) 2233-6656
Journal of Magnetics 19(1), 90-100 (2014) http://dx.doi.org/10.4283/JMAG.2014.19.1.090

FFT-Based Position Estimation in Switched Reluctance Motor Drives

Keunsoo Ha[1], Jaehyuck Kim[2]*, and Jang Young Choi[3]

[1]*Samsung Electro-Mechanics, Suwon, Gyeonggi-Do, Republic of Korea*
[2]*Wonkwang University, Iksan, Jeonllabuk-Do, Republic of Korea*
[3]*Chungnam National University, Daejeon, Republic of Korea*

(Received 30 November 2013, Received in final form 5 February 2014, Accepted 6 February 2014)

Position estimation that uses only active phase voltage and current is presented, to perform high accuracy position sensorless control of a SRM drive. By extracting the amplitude of the first switching harmonic terms of phase voltage and current for a PWM period through Fast Fourier Transform (FFT), the flux-linkage and position are estimated without external hardware circuitry, such as a modulator and demodulator, which result in increased cost, as well as large position estimation error, produced when the motional back EMF is ignored near zero speed. A two-phase SRM drive system, consisting of an asymmetrical converter and a conventional closed-loop PI current controller, is utilized to validate the performance of the proposed position estimation scheme in comprehensive operating conditions. It is shown that the estimated values very closely track the actual values, in dynamic simulations and experiments.

Keywords : switched reluctance motor, position estimation, incremental inductance, first switching harmonic, fast fourier transform

1. Introduction

The switched reluctance motor (SRM) has a simple configuration and winding design, which results in lower cost than classical machines, for the same power [1-3]. Moreover, lower cost converter [4, 5] topologies applied to the machine, as well as the control strategy [6-8] adopted to ensure variable speed operation, makes SRMs very attractive, in variable speed motor applications. In SRM drives, it is necessary to have rotor position information, to determine turn-on and turn-off angles, to excite and commutate the phase windings. Current research has focused on the estimation of rotor position without position sensors, and a large number of position estimation algorithms are broadly classified into four categories in [9]. Table 1 summarizes the features of the various sensorless position estimation algorithms.

The first approach using active phase voltage and current measurement [10-12] does not need any hardware for sensing signals, except for the phase voltage and current. In addition, it does not need any probing pulses. However, it may produce large estimation errors near zero speed, if the motional back EMF is neglected, and improper measurement of the winding resistance will lead to erroneous estimation.

The second approach [13] is to use mutually induced voltage in an inactive phase, in the chopping mode. The mutually induced voltage is very small in magnitude, and appears across the inactive phase; therefore, it is difficult to extract rotor position information, by capturing the mutually induced voltage.

The third approach [14-16] is to use low-level and high frequency signals injected into an inactive phase, to obtain phase inductance variation, which is then mapped to position information. However, the injected signals in these methods need to be low, to minimize negative torque, avoid inter-phase coupling effects, and minimize the volume and cost of external injection circuitry.

The fourth approach [17, 18] is position estimation by intelligent control methods, consisting of fuzzy models and artificial neural network controllers. These methods are not dependent on the magnetic characteristics of the motor, and are thus independent of parameter variations and disturbances. However, a large number of computations for the training of the neural network and many fuzzy rules are required, to have high accuracy position estimation.

©The Korean Magnetics Society. All rights reserved.
*Corresponding author: Tel: +82-63-850-6733
Fax: +82-63-850-6745, e-mail: jaehkim@wku.ac.kr

© 2014 Journal of Magnetics

Table 1. Comparison of various position estimation methods

Methods	Merits	Demerits
Active phase voltage & current measurement	1. No additional hardware, except for circuitry to measure the active phase voltage and current.	1. Neglect of back emf at low speed 2. Resistance error, due to parameter sensitivity or thermal effects.
Mutual voltage measurement	1. Estimates position by simple measurement of mutual voltage, using the relationship between mutual voltage and position.	1. Difficult to extract the mutual voltage, due to small magnitude. 2. External hardware to detect the mutual voltage; e.g. S/H circuit, rectifying circuit, and filter.
External signal injection	1. Estimates position by simple measurements of signal at inactive phase, containing inductance variation.	1. Mutual coupling effect. 2. Negative torque generation. 3. External hardware; e.g. modulator and demodulator. 4. Inductance variation depends on the frequency of injected signal.
Intelligent controls	1. No addition hardware, except for circuitry to measure the active phase voltage and current.	1. A large number of computations for training data and fuzzy rules. 2. Not the preferred approach for simple implementation.

Various techniques suggested in the literature have their own merits and demerits, depending on their principles of operation. Ideally, it is desirable to have a position estimation scheme that uses only terminal measurements, and neither requires additional hardware, nor leads to an erroneous estimation, due to the motional back EMF effect near zero speed, as well as the improper measurement of the resistance of the stator winding. In addition, it is desirable to have a reliable operation over the entire speed, while maintaining a high resolution and accuracy. For overcoming these obstacles, a new position estimation method, using the first switching harmonics of the phase voltage and current through the Fourier series, has been proposed in [9], assuming that the phase voltage and current are continuous, and periodic with the switching frequency.

In a method using the Fourier series in [9], the first switching harmonic component of phase current is computed with the help of the slope of phase current during turn-ON and turn-OFF times, assuming the gradients of phase current are linear in a PWM period. A higher slope of phase current in the hardware implementation leads to easier computations for flux-linkage or inductance in a PWM period. Thus the hard chopping method, one of the methods in PWM control strategies, is selected, in order to obtain a higher slope in the phase current.

On the other hand, the method using the FFT described in this paper, does not utilize the linearized equations and compensation algorithm used in [9], which are not easily obtained in the aligned position and higher speed, due to the decrease of the rate of change of phase current with respect to time. Therefore, the first switching harmonic terms of phase voltage and current are directly calculated from their sampled information at a constant rate, in order to ensure that all the relevant information is contained in the sampled signals. Moreover, the soft chopping method can be employed in the FFT-based method, and this paper also demonstrates the effect of the variation of the incremental inductance at constant rotor position, on the variation of phase current waveform, as the rotor pole moves towards the aligned position.

2. Computation of the First Switching Harmonics of Phase Voltage and Current Using the FFT

The phase voltage and current waveform in this research will be sampled at regular time intervals, as shown in Fig. 1; and the sampled values will be transformed into the frequency domain. T is the PWM period, which is the inverse of the switching frequency, T_s is a sampling frequency, and d is the duty ratio for a PWM period.

2.1. Sampling

To ensure that all the relevant information is contained in the phase voltage and current, they should be captured, by sampling. Thus, if the switching frequency at PWM operation is 5 kHz, it should be sampled at 10 kHz or more, by the Nyquist sampling theorem. The anti-aliasing filter should also provide sufficient attenuation, at frequencies above the Nyquist frequency. Because of the non-ideal response of practical filters, the effective Nyquist frequency is taken as the stop-band frequency. In specifying the anti-aliasing filter, it is useful to take the ADC resolution requirements into account. Thus, a filter would be designed to attenuate the frequencies above the Nyquist frequency, to a level not detectable by the ADC; for example, to less than the quantization noise level. Thus, for a system using a B-bit linear ADC, the minimum stop-band attenuation [19] would typically be,

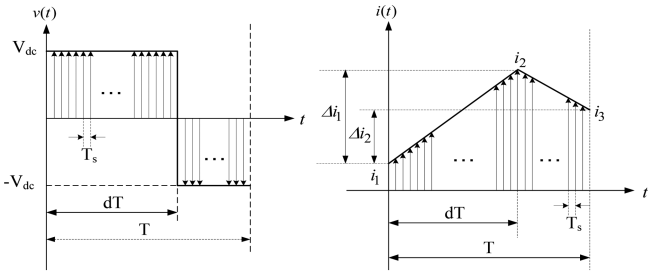

(a) Phase voltage waveform (b) Phase current waveform

Fig. 1. Phase voltage and current waveforms during one PWM period.

$$A_{\min} = 20\log(\sqrt{1.5}\times 2^{B+1}) \tag{1}$$

where, B is the number of bits in the ADC, and $A_{\min}$ is the minimum stop-band attenuation in the low-pass filter. The values of $A_{\min}$ for 10-bit and 12-bit ADC resolutions are 68 dB and 80 dB, respectively.

The use of an analog filter at the front-end of a DSP system also introduces other constraints, such as phase distortion. In order to minimize the phase distortion in the anti-aliasing filters, over-sampling has been introduced in real-time signal processing, so that the transition width is wider, and the phase distortion can be reduced. Therefore, the effective noise power density at the band of interest is lower at higher sampling rates, and this leads to an enhancement of the signal-to-noise ratio.

Assuming that each phase of SRM can be independently driven with the 5 kHz PWM method, and the phase voltage and current of SRM are sampled and acquired with a 12-bit ADC real-time DSP system, the band of interest frequencies extends from 0 to 5 kHz, and the first switching harmonic frequency is 5 kHz. A third-order Butterworth filter can be used, because it has the flattest pass-band region, so that it has the least attenuation over the desired frequency range. Choosing the folding frequency, $F_s/2$ as the effective stop-band frequency, the minimum sampling frequency can then be computed, as

$$-A_{\min} = 20\log(|H(f)|) = 28\log\left(1/\left[1+\left(\frac{f}{f_c}\right)^6\right]^{1/2}\right) \tag{2}$$

where, $A_{\min}$ is the minimum stop-band attenuation, 80 dB for 12-bit ADC resolutions, $H(f)$ and f_c are the gain and cutoff frequency of the third-order Butterworth anti-aliasing filter, and f is the folding frequency, $F_s/2$. From (2), we have $f > 107.7$ kHz $= F_s/2$. Thus the sampling frequency should be greater than 215.4 kHz. Letting $F_s = 250$ kHz, the aliasing level at 5 kHz can be obtained, as

$$\frac{1}{\left[1+\left(\frac{f-F_s}{f_c}\right)^6\right]^{1/2}} = \frac{1}{\left[1+\left(\frac{5-250}{5}\right)^6\right]^{1/2}} = 8.5\times 10^{-6} \tag{3}$$

The level of aliasing error relative to the signal level at 5 kHz can be obtained, as

$$\frac{8.5\times 10^{-6}}{0.7071}\times 100 = 0.0012[\%] \tag{4}$$

2.2. First Switching Harmonics of Phase Voltage and Current

Assume that a waveform has been sampled at a certain regular time interval T, to produce the sample sequence $\{x(nT)\} = x(0), x(t), ..., x[(N-1)T]$ of N sample values, the N-point FFT computation can be represented, as

$$X(k) = \sum_{n=0}^{N-1} x(nT)e^{-j2\pi nk/N} = \sum_{n=0}^{N-1} x(nT)W_N^{kn}$$
$$= \sum_{n=0}^{N-1} x(nT)\left(\cos\left(\frac{2\pi nk}{N}\right) - j\sin\left(\frac{2\pi nk}{N}\right)\right) \tag{5}$$

where, $k = 0, 1, ..., N-1$, and W_N^{kn} is called the twiddle factors. In the implementation of the FFT algorithm on DSP controller, twiddle factors are initialized in memory as SIN and COS values.

In this research, the SRM is controlled at the switching frequency of 5 kHz, and the phase voltage and current are sampled at the rate of 250 kHz, to reduce the aliasing effect in sampling, where the size of FFT (N) is 50 samples, and the first harmonic frequency is given by 5 kHz. Hence 25 values of SIN and 25 values of COS are initialized into a memory of the DSP controller.

Therefore, the amplitude and phase angle of the first harmonic component of phase voltage, $V(1)$, can be expressed as,

$$v_{c1} = \sqrt{(\mathrm{Re}\{V(1)\})^2 + (\mathrm{Im}\{V(1)\})^2},\ v_{\varphi 1} = \tan^{-1}\left(\frac{\mathrm{Im}\{V(1)\}}{\mathrm{Re}\{V(1)\}}\right) \tag{6}$$

where, $V(1)$ is the first harmonic component in the FFT computation of phase voltage, and $\mathrm{Re}\{V(1)\}$ and $\mathrm{Im}\{V(1)\}$ are the real and imaginary parts of $V(1)$, respectively. Similarly, the amplitude and phase angle of the first harmonic component of phase current, $I(1)$, can be expressed, as

$$i_{c1} = \sqrt{(\mathrm{Re}\{I(1)\})^2 + (\mathrm{Im}\{I(1)\})^2},\ i_{\varphi 1} = \tan^{-1}\left(\frac{\mathrm{Im}\{I(1)\}}{\mathrm{Re}\{I(1)\}}\right) \tag{7}$$

where, $I(1)$ is the first harmonic component in the FFT computation of phase current, and $\mathrm{Re}\{I(1)\}$ and $\mathrm{Im}\{I(1)\}$ are the real and imaginary parts of $I(1)$, respectively.

Given phase angles of the first switching harmonic of phase voltage and current in a PWM period, the phase

difference between two instantaneous phase angles in a PWM period can be defined, as

$$\varphi = |v_{\varphi 1} - i_{\varphi 1}| \tag{8}$$

3. Parameter Estimation

3.1. Flux-linkage Estimation

As aforementioned in [9], the inductance of SRM is estimated as in Eq. (9), by using the first switching harmonics of phase voltage and current, and the inductive reactance in the simplified equivalent circuit of SRM, which was originally reported by [20].

$$L_i = \left(\frac{v_{c1}}{i_{c1}} \cdot \frac{T}{2 \cdot \pi} \right) \tag{9}$$

However, if the phase current flowing through a stator winding is controlled by regulated dc current with a small variation ΔI, the phase inductance [9] can be expressed as the ratio of change in flux-linkage to the corresponding change in phase current, and is given, as

$$L_i = \frac{\Delta \lambda}{\Delta I} \tag{10}$$

where, $\Delta\lambda$ is the variation of flux-linkage established by the applied phase current, ΔI is the variation of phase current at the regulating active phase current, and L_i is referred to as the incremental inductance.

In addition, the variation of the incremental inductance at constant rotor position produces variation of the phase current waveform, as the rotor pole moves towards the aligned position, as shown in Fig. 2. This shows the variation of phase current at the unaligned, mid, and aligned positions, when the phase current command is 2 A, and the switching frequency is 5 kHz.

In SRMs, the flux-linkage can be described as the multiplication of the phase current and the self-inductance of the stator winding. Neglecting the mutual inductance between phases, the voltage equation for one phase of the SRM is given, by

$$v(t) = R \cdot i + \frac{\partial \lambda}{\partial i}\frac{di}{dt} + \frac{\partial \lambda}{\partial \theta}\frac{d\theta}{dt} \tag{11}$$

From (11), the rate of change of the phase current with respect to time can be derived, as

$$\frac{di}{dt} = \left\{ v - R \cdot i - \frac{\partial \lambda}{\partial \theta}\frac{d\theta}{dt} \right\} / \frac{\partial \lambda}{\partial i} \tag{12}$$

Considering the nonlinear effects of the saturation, (12) can be expanded, as

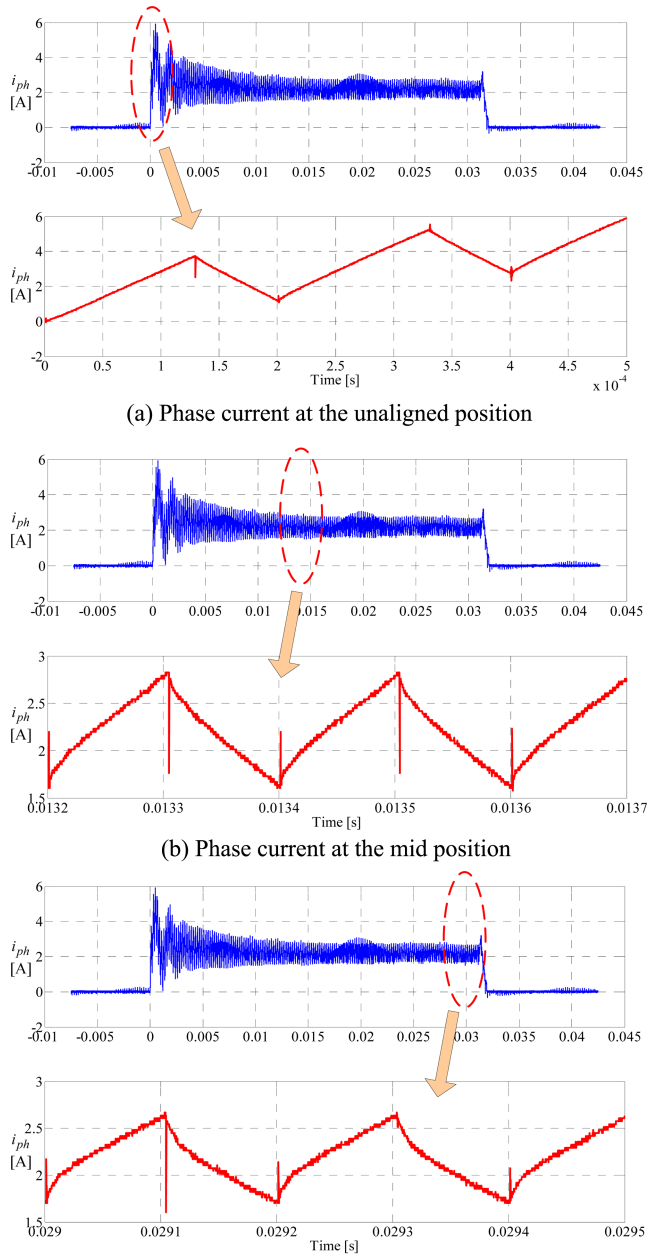

(a) Phase current at the unaligned position

(b) Phase current at the mid position

(c) Phase current at the aligned position

Fig. 2. (Color online) Phase current at the unaligned, mid-point, and aligned positions.

$$\frac{di}{dt} = \left\{ v - R \cdot i - i \cdot \frac{\partial L}{\partial \theta}\frac{d\theta}{dt} \right\} / \left\{ L + i \cdot \frac{\partial L}{\partial i} \right\} \tag{13}$$

When a positive voltage is applied to the stator winding during turn ON, as the rotor pole is moving towards the aligned position, the rate of change of inductance with respect to phase current at a constant rotor position is negative; and the incremental inductance L_i at constant rotor position in the denominator of (12), is lower than the self-inductance L.

$$v > 0,\ \left.\frac{\partial L}{\partial i}\right|_{ON} < 0,\ L_i = \left.\frac{\partial \lambda}{\partial i}\right|_{ON} < L \tag{14}$$

Hence, as the rotor pole is moving towards the aligned position, the rate of change of phase current with respect to time increases during turn ON, as shown in Fig. 2.

On the other hand, while a negative or zero voltage is applied to the stator winding during turn OFF, as the rotor pole is moving towards the aligned position, the rate of change of inductance with respect to phase current at constant rotor position is negative, and the incremental inductance L_i at constant rotor position in the denominator of (12), is lower than the self-inductance L.

$$v \le 0,\ \left.\frac{\partial L}{\partial i}\right|_{OFF} < 0,\ L_i = \left.\frac{\partial \lambda}{\partial i}\right|_{OFF} < L \tag{15}$$

Hence, as the rotor pole is moving towards the aligned position, the rate of change of phase current with respect to time decreases during turn OFF, as shown in Fig. 2. Therefore, this incremental inductance or the variation of flux-linkage is not used for estimating the rotor position, since the variation of the incremental inductance with respect to rotor position is too small to estimate the rotor position, as the rotor moves towards the aligned position. This makes it difficult for position estimation to be useful in SRM.

In order to overcome this drawback, the incremental inductance is converted into a flux-linkage or self-inductance to be compatible with FEA results, resulting in estimating an accurate rotor position at the region. Flux-linkage is chosen in this research, and how to convert into flux-linkage is presented in detail in [9]. Based on [9], the flux-linkage in a PWM period can be given repeatedly, during every PWM period, as

$$\lambda_{n+1} = a_n \cdot (1-2d_n) \cdot T + \lambda_n \tag{16}$$

where, λ is the flux-linkage, and a is the slope of flux-linkage with respect to time, during turn ON.

3.2. Position Estimation

Fig. 3 shows the magnetization characteristic of the two-phase 6/3 SRM [21] used in this research. In [21], the flux-linkage starts to saturate from 4A, and is periodic, with a period of 120º. If at a given instant, the estimated flux-linkage and the phase current of particular phase are known, then from the stored flux-linkage characteristics of the SRM, the rotor position will be found, provided it is also known whether the operating mode is motoring or braking. The block diagram for the proposed position estimation using FFT is represented in Fig. 3.

4. Dynamic Simulation Results

Position estimation, using the first switching harmonics of phase voltage and current decomposed by FFT, is simulated, by using Matlab. Several simulations at different currents commands have been executed, to prove the validity of the proposed position estimation algorithm, under various loads. Note that no speed control loop is included. In dynamic simulations, the symmetrical PWM method with a fixed frequency (set at 5 kHz) is employed for dynamic current control. The asymmetric bridge converter is designed to apply a phase voltage in hard-chopping mode, to increase the rate of the change of phase current for a PWM period. Magnetization data obtained from FEA, which was verified in [21], are stored in a lookup table. The load is applied to the machine from start-up condition. Voltage drops and switching transients of power electronic devices are negligible, compared to the DC-

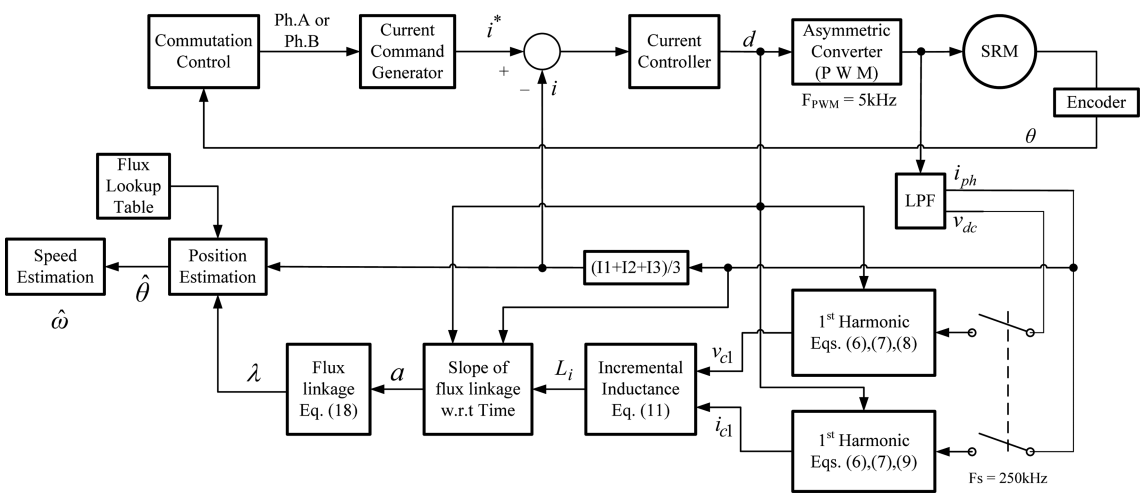

Fig. 3. Block Diagram for the proposed position estimation method.

Table 2. Simulation results at various current commands, under no load

Iref [A]	Average Speed [rpm]	Position Error [deg (°)] $\lvert\Delta\theta\rvert$		Speed Error [rpm] $\lvert\Delta\omega\rvert$		Flux-linkage Error [%] $(\lvert\Delta\lambda\rvert/\lambda_{FEA})\times100$	
		Avg.	Max.	Avg.	Max.	Avg.	Max.
2	Startup	0.0062	0.0152	0.0629	0.1621	0.2254	2.3598
	240	0.1352	0.1575	0.1127	0.3303	0.3856	1.0093
	324	0.1863	0.2093	0.1001	0.4978	0.5120	1.3101
	549	0.3178	0.3405	0.0871	1.1982	0.8843	2.1913
	710	0.4113	0.4360	0.0854	0.8430	1.1216	2.8505
3	Startup	0.0031	0.0079	0.1737	0.3078	0.1281	4.6618
	499	0.3239	0.9031	0.3450	3.8829	0.8843	5.5768
	699	0.4356	0.6878	0.3083	5.7373	1.1615	5.1642
	965	0.5879	0.8077	0.3617	6.0887	1.5312	4.6199
	1133	0.6738	0.9088	0.4742	6.2624	1.7816	4.4957
4	Startup	0.0087	0.0209	0.2961	0.5074	0.0891	1.4535
	745	0.4254	1.4360	0.4639	9.6199	1.1340	8.8252
	988	0.5705	1.5611	0.5644	9.7513	1.4838	10.4247
	1212	0.6895	1.6168	0.9029	11.1730	1.7559	10.8173
5	Startup	0.0129	0.0332	0.4631	0.7687	0.0958	1.3158
	755	0.4578	1.8503	1.0923	14.4914	1.2120	11.0586
	1092	0.6407	2.1789	1.1748	16.5782	1.7013	11.6556
6	Startup	0.0126	0.0267	0.6962	1.3550	0.0946	1.9262
	897	0.3986	2.1473	0.9867	10.8062	1.1806	12.3796
	1360	0.6500	2.7719	1.8058	16.3356	1.9374	16.1274

link voltage and mechanical time constant of the motor.

4.1. No Load Test

The SRM is initially at standstill and no load, when a reference current command is applied, and it runs with phase current regulation. Note that in these simulations, no speed control loop is included. At the rate of 5 kHz, the estimated and actual values of flux-linkage, rotor position, and speed are obtained during 400 PWM cycles at different operating conditions, such as transient startup, as well as low and high speeds. The average and maximum values of the results obtained during 400 PWM cycles are presented in Table 2. Fig. 4 shows the estimated and actual values of the flux-linkage, rotor position and speed at startup, when applying the phase current command of 3A, under no load.

4.2. Load Test

The SRM is initially at standstill with various loads, when a phase current command is applied, and it runs with phase current regulation. Note that no speed loop is included. The SRM runs at 25%, 50%, 75%, and 100% of full load, which is 4 N·m for the prototype. At the rate of 5 kHz, the estimated and actual values of the flux-linkage, rotor position, and speed are obtained during 300 PWM cycles, at different operating conditions. The average and maximum values of the results obtained during 300 PWM cycles are presented in the following Table 3. Fig. 5 shows the estimated and actual values of the flux-linkage, rotor position and speed, when applying the phase current command of 13A, under full load, 4Nm.

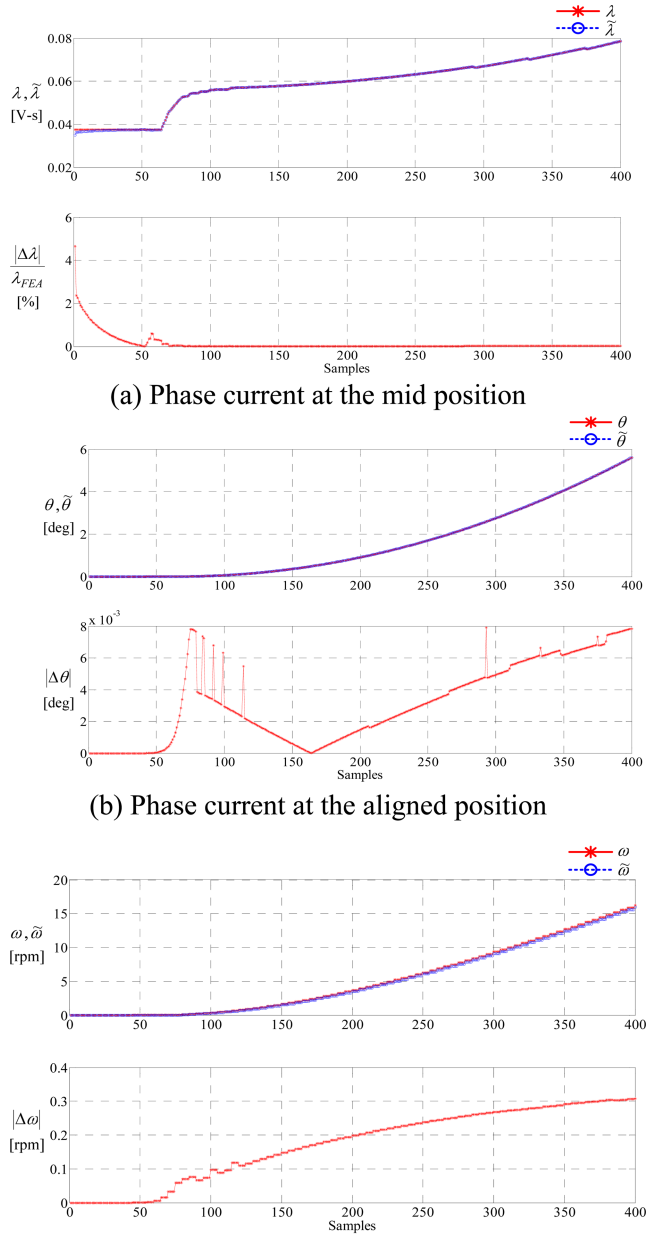

Fig. 4. (Color online) Simulation results at startup and $I^* = 3A$, under no load.

Table 3. Simulation results at various current commands, under various loads

Torque [N·m]	Iref [A]	Avg. Speed [rpm]	Position Error [deg(°)] $\lvert\Delta\theta\rvert$		Speed Error [rpm] $\lvert\Delta\omega\rvert$		Flux-linkage Error [%] $(\lvert\Delta\lambda\rvert/\lambda_{FEA})\times100$	
			Avg.	Max.	Avg.	Max.	Avg.	Max.
1	7	845	0.3387	1.2054	1.5104	8.4918	1.2123	10.9599
2	9	926	0.3409	1.4029	1.3833	17.1263	1.1833	12.3852
3	11	892	0.2537	1.6964	1.8885	18.4599	1.0794	15.4845
4	13	820	0.1890	1.7476	1.6967	16.9927	1.0091	14.3954

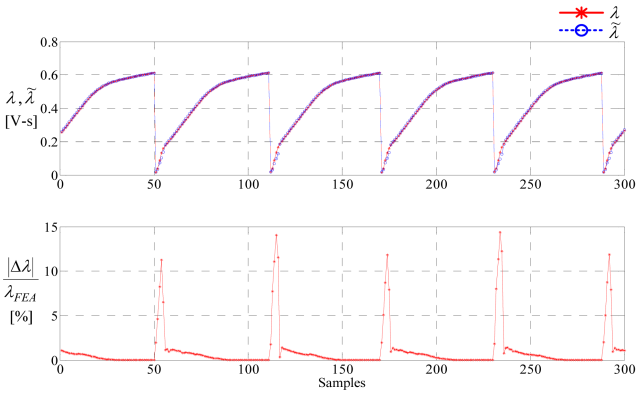

(a) Phase current at the mid position

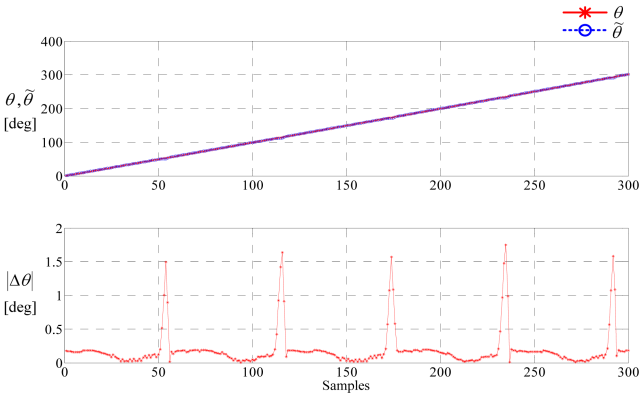

(b) Phase current at the aligned position

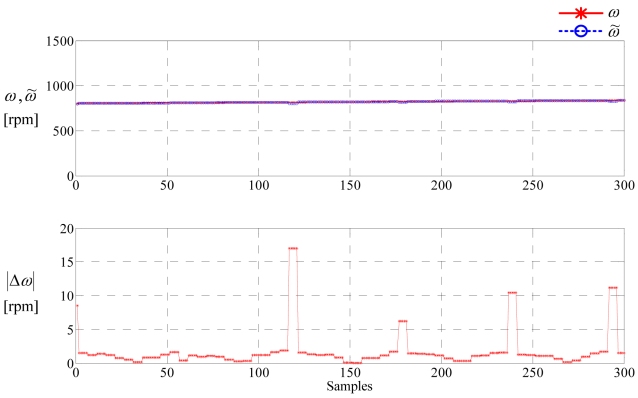

(c) Speed estimation

Fig. 5. (Color online) Simulation results at ω = 820 rpm and I^* = 13A, under full load, 4 Nm.

5. Experimental Evaluation

The implementation of the proposed estimation algorithm using FFT is accomplished, using a classical asymmetric bridge converter. A 16-bit DSP controller of Texas Instruments is employed, in order to implement the proposed algorithm. The DC bus voltage and phase current are sampled at a sampling rate of 250 kHz, and the sample size of FFT computation is 50 samples in a PWM period. From FFT computation of the sampled DC bus voltage and phase current, with the duty cycle provided from the current control loop, the real and imaginary parts of the first switching harmonic of phase voltage and current are calculated.

Based on real and imaginary parts of the first switching harmonics of the phase voltage and current, the flux-linkage is estimated in a PWM period. The flux-linkage values given by FEA are stored into the two-dimensional lookup table, with phase current for row, and rotor position for column. By using linear interpolation in the two-dimensional flux-linkage lookup table, with the estimated flux-linkage and average phase current, the rotor position is estimated. 3-phase AC power supply is fed to a full-bridge rectifier, and a rotary encoder with the resolution of 1024 [pulses/rev] is coupled to the rotor shaft, for evaluating the accuracy of the estimated rotor position. 2.2 hp, two-phase 6/3 SRM is loaded, using a separately excited DC generator coupled to its shaft; and different loads are set, by changing the load resistance, through sliding the knob of a rheostat. The experimental SRM drive system is shown in Fig. 6.

5.1. No Load Test

With the experimental setup described in Fig. 6, the proposed position estimation scheme using FFT is performed at different phase current commands, under no load. The SRM is initially at standstill with no load, when a phase current command is applied to the SRM, and it runs with phase current regulation. Note that no speed control loop is included. At the rate of 5 kHz, the estimated and actual values of the flux-linkage, rotor position,

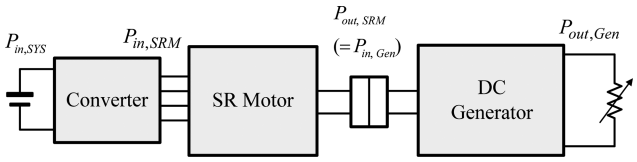

Fig. 6. Experimental Setup.

Table 4. Experimental results at various current commands, under no load

Iref [A]	Average Speed [rpm]	Position Error [deg (°)] $\lvert\Delta\theta\rvert$		Speed Error [rpm] $\lvert\Delta\omega\rvert$		Flux-linkage Error [%] $(\lvert\Delta\lambda\rvert/\lambda_{FEA})\times100$	
		Avg.	Max.	Avg.	Ma.	Avg.	Max.
2	Startup	0.4518	0.7184	1.4755	2.8809	2.6341	4.1716
	236	0.1881	0.4822	1.8480	6.3790	0.7363	5.5064
	314	0.2577	0.8943	3.2245	11.0724	1.0801	9.4785
	590	0.5922	1.2854	8.3459	27.1738	2.1589	11.0761
	774	0.6238	1.6743	10.7887	25.1936	2.3061	13.6797
3	Startup	0.4425	0.8671	1.5727	3.6999	2.3017	3.8532
	490	0.4068	1.2421	5.9109	19.4738	1.5823	11.0161
	676	0.6442	1.3548	11.0311	30.2657	2.3562	12.2106
	941	0.6094	2.0893	10.1536	30.9586	2.4360	17.0758
	1144	0.8561	1.9715	13.0675	24.5110	3.3168	18.3464
4	Startup	0.1976	0.7256	1.6048	5.1568	0.8927	2.3535
	705	0.6342	1.5586	9.9982	24.3159	2.3329	14.2513
	976	0.7128	1.5190	10.8604	25.1939	2.9084	15.8663
	1189	0.9549	1.8449	14.3880	25.3826	3.8394	16.5392
5	Startup	0.0875	0.4255	1.0851	3.3632	0.3692	1.3069
	724	0.6040	1.4314	10.1744	22.2554	2.1913	13.5979
	1085	0.8747	1.8458	15.2846	31.1438	3.1725	18.6625
6	Startup	0.5617	1.9575	3.4674	10.9815	1.5013	4.2524
	874	0.7247	1.6199	12.3772	33.4202	2.6855	15.4853
	1280	0.9641	2.0968	16.6907	37.5575	3.6249	18.8666

and speed are obtained during 400 PWM cycles at different operating conditions, due to the lack of the available memory space of the DSP controller. The average and maximum values of the results obtained during 400 PWM cycles are summarized in Table 4.

Fig. 7 shows the estimated and actual values of the flux-linkage, rotor position and speed at startup and high speed, when applying the phase current command of 3A, under no load.

From Table 4 and Fig. 7, the average and maximum errors of the flux-linkage, position, and speed are approximately 2.30% and 3.85%, 0.44deg and 0.86deg, and 1.57 rpm and 3.69 rpm, respectively. It can be observed that the proposed position estimation scheme using FFT works reliably at different operating conditions, under no load.

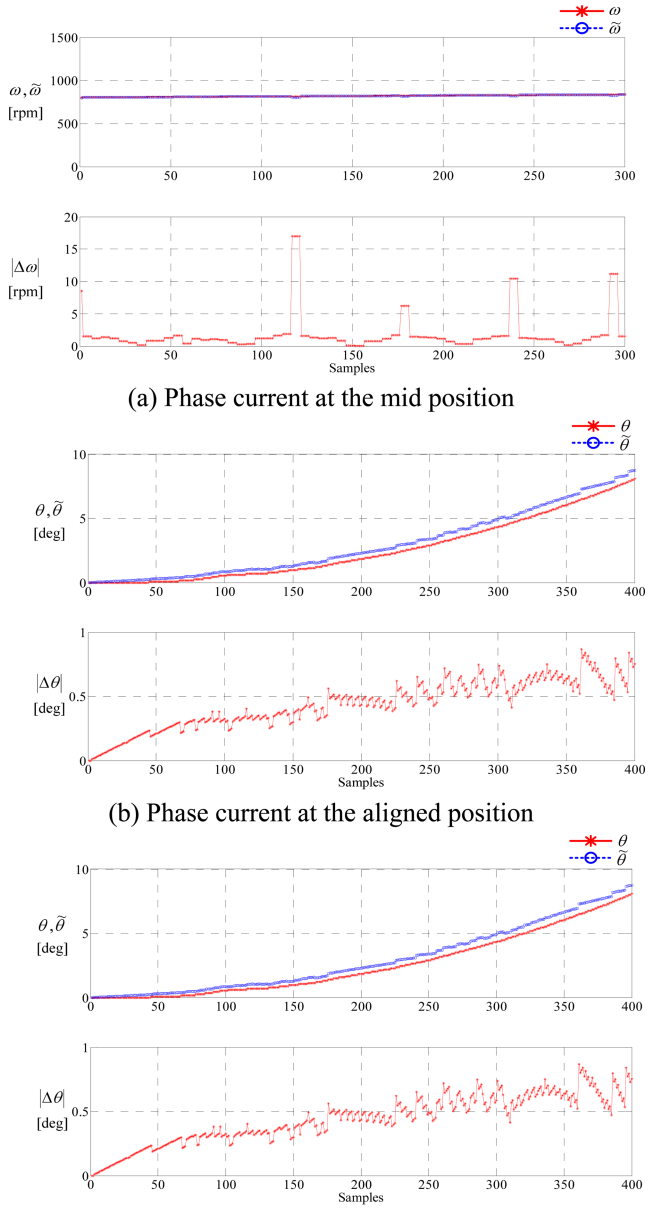

(a) Phase current at the mid position

(b) Phase current at the aligned position

(c) Speed estimation

Fig. 7. (Color online) Simulation results at startup and $I^* = 3A$, under no load.

5.2. Load Test

In order to validate the performance of the proposed position estimation scheme using FFT in a more comprehensive operating condition, various experiments are performed at different phase current commands, under various loads. The load generated from a separately excited DC generator is fed into the SRM coupled to its shaft. The SRM runs at 25%, 50%, 75%, and 100% of full load, which is 4 N·m for the prototype SRM. Higher current commands of more than 7A are applied to the SRM for reliable startup, since the SRM cannot recover from stall-

Table 5. Experimental results at different current command, under various loads

Torque [N·m]	Iref [A]	Avg. Speed [rpm]	Position Error [deg(°)] $\lvert\Delta\theta\rvert$		Speed Error [rpm] $\lvert\Delta\omega\rvert$		Flux-linkage Error [%] $(\lvert\Delta\lambda\rvert/\lambda_{FEA})\times100$	
			Avg.	Max.	Avg.	Max.	Avg.	Max.
1	7	864	0.6960	1.5221	11.2061	26.6586	2.5967	13.1478
2	9	889	0.8884	1.5678	14.4563	25.5034	2.9398	16.5401
3	11	853	0.8369	1.6458	11.1746	27.9180	2.8596	13.6750
4	13	819	0.7842	1.6916	9.6338	23.2913	2.5371	13.4636

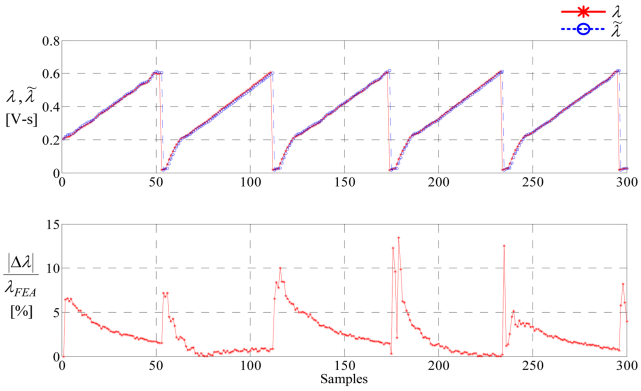

(a) Phase current at the mid position

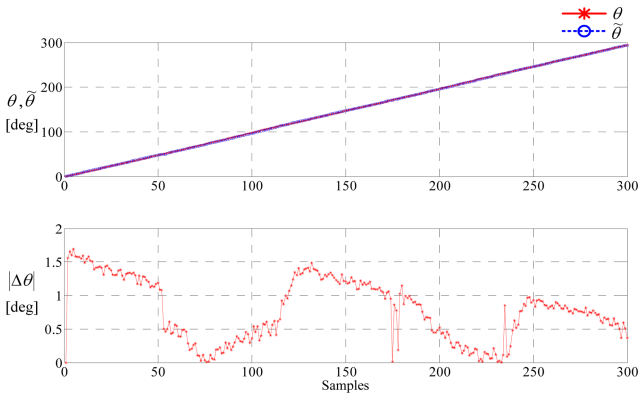

(b) Phase current at the aligned position

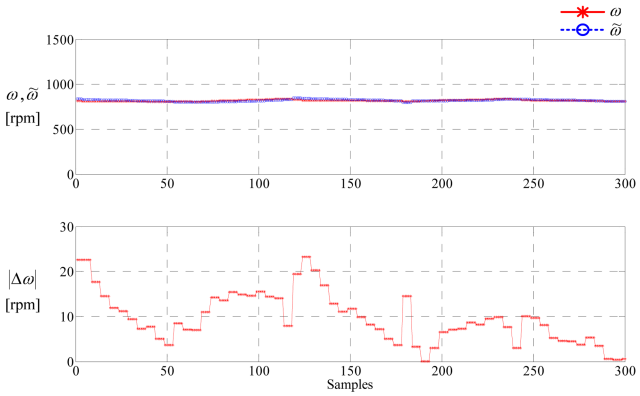

(c) Speed estimation

Fig. 8. (Color online) Experimental results at ω = 819 rpm and I^* = 13A, under full load, 4 Nm.

ing at lower current less than 7A, by its torque performance [21]. The SRM is initially at standstill, and no speed control loop is included. In order to reduce the position error in the saturated region, the flux-linkage profile, linearly varying with respect to the rotor position from the unsaturated to saturated region, is stored into a DSP memory. At the rate of 5 kHz, the estimated and actual values of the flux-linkage, rotor position, and speed are obtained during 300 PWM cycles at different operating conditions, due to the lack of the available memory space of the DSP controller. The average and maximum values of the results obtained during 300 PWM cycles are summarized in Table 5.

Fig. 8 shows the estimated and actual values of the flux-linkage, rotor position and speed, when applying the phase current command of 13A, under full load, 4Nm.

From Table 5 and Fig. 8, the average and maximum errors of the flux-linkage, position, and speed are approximately 3.26% and 16.30%, 0.90deg and 1.74deg, and 10.90 rpm and 23.63 rpm, respectively. The flux-linkage error increases around the unaligned position, due to the higher rate of change of phase current, causing the increase of the position and speed error. However, the position error tends to decrease when the rotor is moving towards the aligned position, due to getting rid of the nonlinear effects of the saturation.

6. Analysis

In this research, experimental verification of the proposed position estimation scheme using the FFT has been carried out. The SRM has been started up from zero speed, at different current commands, under various loads, and it has run with phase current regulation. The loads of 25%, 50%, 75%, 100% of the rated load, 4 N·m, have been applied to the SRM, by switching a resistive load, which is connected to a DC generator. The rotor position is set to zero, at the aligned position. Note that no speed control loop is included, and each phase is excited with the fixed conduction angle, regardless of the current command and rotor speed. The conduction angle of 60° is used, and the

Table 6. Comparison of results of experiments and simulations

Tor [Nm]	Iref [A]	Position Error [deg]				Speed Error [rpm]				Flu-linkage Error [%]			
		Experiment		Simulation		Experiment		Simulation		Experiment		Simulation	
		Avg.	Max.	Avg.	Max.	Avg.	Max.	Avg.	Max.	Avg.	Max.	Avg.	Max.
0	2	0.47	1.09	0.21	0.23	5.57	14.31	0.08	0.56	2.08	8.84	0.65	2.23
	3	0.61	1.46	0.38	0.58	7.89	18.36	0.33	3.93	2.58	11.87	1.03	4.76
	4	0.60	1.36	0.40	1.05	8.80	18.43	0.57	7.12	2.45	11.31	1.05	7.30
	5	0.52	1.23	0.37	1.35	8.84	18.92	0.91	10.61	1.91	11.18	1.00	8.01
	6	0.75	1.88	0.35	1.65	10.84	27.32	1.16	9.50	2.60	12.86	1.07	10.14
1	7	0.69	1.52	0.33	1.20	11.20	26.65	1.51	8.49	2.59	13.14	1.21	10.95
2	9	0.88	1.56	0.34	1.40	14.45	25.50	1.38	17.12	2.93	16.54	1.18	12.38
3	11	0.84	1.64	0.25	1.69	11.17	27.91	1.88	18.45	2.85	13.67	1.07	15.48
4	13	0.78	1.69	0.18	1.74	9.63	23.29	1.69	16.99	2.53	13.46	1.00	14.39

rotor speed range has the limitation of being lower than 1,500 rpm in the experiments. This is due to the tail current, which flows into the negative inductance slope region, after commutating the excited phase [22]. The correlation between the dynamic simulations and experiments of the proposed position estimation scheme using the FFT is provided in Table 6.

It can be pointed out from Table 6 that the maximum position errors in experiments are slightly smaller, than in simulations at high current references, since the flux-linkage is linearly varying with respect to the rotor position, from phase excitation to commutation angle. On the other hand, the average rotor position errors in experiments are slightly larger, than in simulations. This is because the shifted phase current due to an anti-aliasing LPF, and the propagation delay time of devices linked to ADC channels of the DSP [23], which is approximately 24 μs in the developed drive system, are sampled without any compensation for correcting the shifted phase current; while the shifted phase current is compensated by a linear least squares (LLS) fitting algorithm in the position estimation scheme, using the Fourier series in [9]. Nevertheless, rotor position errors in the experiments are less than 2 deg, and the rotor position is therefore reliably estimated in a PWM period.

In spite of the accurate estimation of the rotor position in experiments, the rotor speed error is larger, compared to that in simulations. This is attributed to the different selection of the filter coefficient, to filter out the estimated rotor speed in the experiments. In simulations, the filter coefficient is set to 0.95; while it is set to 0.9 in the experiments, because the rotor position error in the experiments is smaller than in the simulations.

From a thorough analysis, it can be demonstrated that the experimental results are very close to the simulation results, and the performance of the proposed position estimation method using FFT has satisfactory results, which leads to a reliable operation at different operating conditions, such as transient startup, as well as low and high speeds under various loads, without position sensors.

Table 7. Computation time on DSP for the proposed position estimation algorithm [unit: μs]

Items	Fast Fourier Transform (sample size = 50)
First switching harmonics computation	92.8
Flux-linkage estimation	11.8
Rotor position estimation	11.8
Rotor speed estimation	1.4

In order to measure the computational burden for the proposed algorithm in the experiments, the execution time to conduct the proposed algorithm on the DSP controller is measured, and given in the following Table 7. The proposed FFT-based position estimation algorithm spends 92.8 μs to compute the first switching harmonics of the phase voltage and current in a PWM period. In this paper, only the first switching harmonic components are required, and the proposed position algorithm using the FFT is reasonable, and suitable for implementation.

7. Conclusions

In this research, a new position estimation method using the first switching harmonics of phase voltage and current through the FFT has been presented, to perform high accuracy position estimation for SRM. In the FFT-based position estimation algorithm, the shifted phase current is sampled without any compensation for correcting it [9], and thereby the flux-linkage estimated from the phase voltage and current has large errors, resulting in increasing the rotor position error. The combination of the pro-

posed method and back-EMF methodology only in the high speed region, however, could improve the estimation accuracy, with increasing the sampling frequency and sample size into a higher speed DSP controller.

In order to validate the performance of the proposed position estimation scheme using the FFT, it has been analyzed, and a comprehensive set of simulations and experiments have been accomplished and verified, with a two-phase 6/3 SRM drive system. From the correlation between the experiments and simulations, it is evident that the proposed position estimation method using the FFT is sufficiently accurate, and works satisfactorily at various operating points, such as startup, and low and high speeds, under various loads. However, it has the disadvantage that it is difficult to work in single pulse operation mode, where the SRM operates at higher speeds and there is no time for chopping to take place.

Acknowledgement

This research was supported by Basic Science Research Program through the National Research Foundation of Korea (NRF-2012R1A1A1015767) and was also supported by Industry, University and Research Institute Core Technology development & Industrialized Supporting Business through Jeonbuk province in 2013.

References

[1] R. Krishnan, ICEMS. International Conference on, 472 (2007).
[2] A. Tenconi, F. Profumo, S. E. Bauer, and M. D. Hennen, IEEE Trans. Ind. Electron. **55**, 3619 (2008).
[3] P. C. Desai, M. Krishnamurthy, N. Schofield, and A. Emadi, IEEE Trans. Ind. Electron. **57**, 649 (2010).
[4] N. McNeill, D. Holliday, and P. H. Mellor, IEEE Trans. Power Electron. **24**, 548 (2009).
[5] C. R. Neuhaus, N. H. Fuengwrodsakul, and R. W. D. Doncker, IEEE Trans. Power Electron. **23**, 2257 (2008).
[6] Y.-C. Chang and C.-M. Liaw, IEEE Trans. Power Electron. **23**, 445 (2008).
[7] J.-Y. Chai, Y.-C. Chang, and C.-M. Liaw, IEEE Trans. Power Electron. **25**, 1135 (2010).
[8] I. Kioskeridis and C. Mademlis, IEEE Trans. Power Electron. **24**, 301 (2009).
[9] K. Ha, R. Kim, and R. Krishnan, IEEE Trans. Ind. Electron. **58**, 5352 (2011).
[10] H. Abootorabi Zarchi, J. Soltani, and G. Arab Markadeh, IEEE Trans. Ind. Electron. **57**, 375 (2010).
[11] G. Foo and M. F. Rahman, IEEE Trans. Ind. Electron. **57**, 1270 (2010).
[12] C. J. Bateman, B. C. Mecrow, A. C. Clothier, and P. P. Acarnley, IEEE Trans. Ind. Appl. **46**, 2329 (2010).
[13] I. Husain and M. Ehsani, IEEE Trans. Ind. Appl. **30**, 665 (1994).
[14] K. R. Geldhof, A. P. M. Van den Bossche, and J. A. Melkebeek, IEEE Trans. Ind. Electron. **57**, 2954 (2010).
[15] G. Pasquesoone, R. Mikail, and I. Husain, IEEE Trans. Ind. Appl. **47**, 1724 (2011).
[16] C. Jun and D. Zhiquan, IEEE Trans. Power Electron. **27**, 3410 (2012).
[17] Z. Lin, D. Reay, B. Williams, and X. He, IET Electric Power Appl. **4**, 67 (2010).
[18] L. O. Henriques, L. G. Rolim, W. I. Suemistu, J. A. Dente, and P. J. Branco, IEEE Trans. Power Electron. **26**, 3330 (2011).
[19] E. C. Ifeachor and B. W. Jervis, Digital Signal Processing - A Practical Approach, 1993.
[20] M. Wellner and R. Krishnan, Property of Virginia Tech. (2003).
[21] S. G. Oh and R. Krishnan, IEEE Trans. Ind. Appl. **43**, 1247 (2007).
[22] D.-H. Lee, J. Liang, Z.-G. Lee, and J.-W. Ahn, IEEE Trans. Ind. Electron. **56**, 3021 (2009).
[23] TMS320x280x, 2801x, 2804x DSP Analog-to-Digital converter: Texas Instruments (2005).